7 6

J. Electroanal. Chem., 127 (1981) 43–58
Elsevier Sequoia S.A., Lausanne—Printed in The Netherlands

SEMICONDUCTOR ELECTRODES

PART 38. PHOTOELECTROCHEMICAL BEHAVIOR OF n- AND p-TYPE GaAs ELECTRODES IN TETRAHYDROFURAN SOLUTIONS

F. DI QUARTO * and ALLEN J. BARD

Department of Chemistry, University of Texas at Austin, Austin, TX 78712 (U.S.A.)

(Received 19th January 1981; in revised form 6th April 1981)

ABSTRACT

The photoelectrochemical behavior of n- and p-type GaAs was investigated in tetrahydrofuran solutions containing different redox couples. From the impedance measurements at different frequencies the flat-band potentials were located at approximately −1.0 (±0.1) V vs. SCE for n-GaAs and at 0.0 (±0.1) V vs. SCE for p-GaAs electrodes. Under illumination both anodic (at n-GaAs) and cathodic (at p-GaAs) photocurrents were observed, with redox couples located outside the band gap of the semiconductor. The measured photovoltage was linearly dependent upon the potential of the redox couple located within the band gap of the semiconductor. The photovoltage became constant, with couples lying below the valence band edge (at n-GaAs) or above the conduction band edge (at p-GaAs). The results are explained by inversion layer formation or pinning.

INTRODUCTION

The use of organic solvents in the study of the photoelectrochemical (PEC) behavior of semiconductor electrodes offers several advantages with respect to aqueous electrolyte solutions [1,2]. The wide potential range of solvent stability permits the use of numerous one-electron reversible redox couples spanning a wide range of redox potentials. Moreover, improved resistance toward the photodissolution process can be expected in organic solvents because of the smaller solvation energy for the dissolution products when compared with aqueous solutions [3,4]. This last advantage is particularly useful in the study of a small band-gap semiconductor like GaAs which shows a very complex behavior in aqueous solutions owing to the formation of surface layers of different nature depending on the history of the electrode [5–11].

Although the use of special redox couples like selenide/polyselenide have been shown to suppress the photodissolution of the GaAs electrodes in aqueous solutions [12–14], organic solvents are still of interest in studies of the kinetics of the electron-transfer process at the semiconductor electrode/electrolyte interface for couples covering a wide range of redox potentials, and in the discovery of alternative

* Permanent address: Istituto di Ingegneria Chimica, Viale delle Scienze, 90128 Palermo, Italy.

electrolyte systems for PEC cells. Previous studies from this laboratory have demonstrated the value of using different redox couples in acetonitrile to locate the energy levels of semiconductors (e.g. the conduction band (CB) edge, E_c; the valence band (VB) edge, E_v) as well as information about the existence of surface energy levels (surface states) in the band gap [2,15–18]. On the basis of these experimental results as well as previous theoretical and experimental work, it is clear that the solvent plays a major role in determining the nature of the energetics of the semiconductor/electrolyte interface [19,20].

This study of the photoelectrochemical behavior of both n-type and p-type GaAs electrodes in tetrahydrofuran (THF) electrolyte solutions was aimed at obtaining further information about the existence of surface states at the semiconductor/electrolyte interface, about the role played by these energy levels on the kinetics of charge transfer between species in solution and about the energetics at the interface.

EXPERIMENTAL

Single crystals of n-GaAs ($N_D = 10^{17}-10^{18}$ cm^{-3}) with the (111) face exposed to the solution were provided with ohmic contacts by depositing indium on the back side and heating for 2 h in a hydrogen atmosphere at 450°C. A copper wire was attached to the indium with silver conductive paste which was covered with a 5 min epoxy resin. The ohmic contact to the p-type single crystals ($N_A = 4 \times 10^{16}$ cm^{-3}) with the (100) face exposed to the solution was made by depositing a gold layer on the back side and attaching a copper wire with silver paste. The contact was again covered with epoxy resin. The n- and p-type electrodes were polished with 0.5 μm alumina powder, cleaned ultrasonically in methanol and finally rinsed with acetone. They were then mounted in glass tubes with an insulating epoxy resin (Torr-Seal; Varian Assoc., Palo Alto, CA) and finally etched. The etching procedure was as follows: the GaAs was anodically oxidized in H_3PO_4 solutions (pH = 2.5) up to 100 V, followed by dissolution of the anodic oxide in $NH_3:H_2O$ (1 : 1 by volume). This procedure was repeated with each new electrode several times until a layer of GaAs of about 1000 nm was removed for both p- or n-type electrode [21]. An alternative etching procedure for n-type electrodes consisted of chemical attack in $H_2SO_4:H_2O_2:H_2O$ (3 : 1 : 1 by volume) solution. The specimens after etching showed a mirror-like surface, but good reproducibility of the surface morphology was obtained only with the specimens etched by the anodic oxidation procedure.

The THF was stored for several days in a flask containing hydride and was then distilled under vacuum into a flask with a predeposited sodium mirror. After distillation from this flask, the THF was stored in a glove box. All the chemicals employed were used, after purification or in the purest form commercially available, after drying under vacuum. However, a check of the purity of all chemicals used was performed by cyclic voltammetry at a Pt disk electrode at the beginning of each experiment. This procedure was also used to calibrate the reference electrode potential. Polarographic grade tetra-n-butylammonium perchlorate (TBAP), which was dried for three days under vacuum, was used as the supporting electrolyte at 0.2 M concentration.

A three-compartment electrochemical cell was used. The counter-electrode was a platinum foil separated from the test compartment by a medium-porosity glass frit. The quasi-reference electrode was a silver wire immersed in the solution and separated from the working electrode compartment by a low-porosity glass frit. All electrode potentials are reported vs. the aqueous saturated calomel electrode (SCE). A large area (> 10 cm^2) Pt foil counter-electrode immersed in the same compartment as the working electrode was used in impedance measurements.

A P.A.R. 173 potentiostat and P.A.R. 175 universal programmer (Princeton Applied Research Corp., Princeton, NJ) equipped with a Model 2000 X–Y recorder (Houston Instruments, Austin, Texas) were used to obtain the cyclic voltammograms as well as for impedance measurements. In these latter experiments a lock-in amplifier technique, which yields the in-phase and the out-of-phase component of an ac signal superimposed on the triangular sweep, was used. The ac signal (10 mV peak-to-peak) at different frequencies and its components (at 0 and 90°) were obtained by using a P.A.R. model HR-8 lock-in amplifier equipped with an internal oscillator. Because of the high solution resistance, reported voltammetric peak potentials contain some uncompensated ohmic drop.

The light source (632.8 nm; 1.6 mW) for all the experiments was a He–Ne laser. The solutions were prepared and sealed in a helium-filled Vacuum Atmosphere Corporation (Hawthorne, CA) glove box.

RESULTS

Impedance measurements

The impedance of the semiconductor/electrolyte interface was measured as a function of the electrode potential and frequency, ω. The range of frequencies investigated was 70 Hz–5 kHz for n-type and 70 Hz–15 kHz for p-type. The range of potentials swept affected the shapes of the capacitance vs. potential (C_p vs. V) plots. A large amount of hysteresis was found at all frequencies when a large potential range was investigated. Analogous behavior has been reported for experiments performed in aqueous solutions [9,11]. An increase in the scan rate, at fixed ω, from 10 to 500 mV s^{-1} was effective in reducing the hysteresis. An increase in the frequency of the ac signal at fixed scan rate (10 mV s^{-1}) also decreased the amount of hysteresis, but to a lesser extent. However, the most effective method of reducing the hysteresis of the C_p vs. V plots was to reduce the potential range for the impedance measurements to about 0.8 V for both n- and p-type electrodes. All of the quantitative analysis of the impedance measurements reported in the following pertains to such a restricted potential range.

The analysis of the experimental results has been performed by assuming that the C_p measured by the lock-in technique is the space-charge capacitance of the semiconductor, C_{sc}. This assumption implies that (a) there is no contribution to the measured impedance by surface states in the range of electrode potentials investigated; (b) an appreciable faradaic contribution to the measured impedance is

absent; and (c) the condition $\omega^2 R_{s,eq}^2 C_{s,eq}^2 \ll 1$ applies; where $R_{s,eq}$ and $C_{s,eq}$ are respectively the equivalent series resistance and the equivalent series capacitance of the semiconductor/electrolyte interface. If these conditions are satisfied and the Helmholtz double-layer capacitance, C_H, is much larger than C_{sc}, the Schottky–Mott (S–M) equation can be used. The expression of the space-charge capacitance of the semiconductor/electrolyte interface in the depletion region is then [22]

$$1/C_p^2 = 1/C_{sc}^2 = (2/\epsilon\epsilon_0 e N_D)(V - V_{fb} - kT/e) \tag{1}$$

where ϵ is the relative dielectric constant, ϵ_0 the permittivity of free space, e the electronic charge, N_D the doping level and V_{fb} the flatband potential.

The S–M plots for n- and p-type electrodes at different frequencies are shown in Fig. 1. A detailed analysis of the equivalent circuit at different frequencies demonstrated that the assumptions are reasonably satisfied over the potential range investigated at frequencies below ~500 Hz for n-type and ~5 kHz for p-type electrodes. Within these frequency ranges, the S–M plots were straight lines. For the n-type electrodes, the S–M plots were not appreciably affected by different surface treatments. However, electrodes with an anodically formed oxide layer (~10 nm) showed intersection voltages in the S–M plots at much more negative potentials. A similar effect, but to a smaller extent, was observed if the electrode was kept in air for a day after chemical etching.

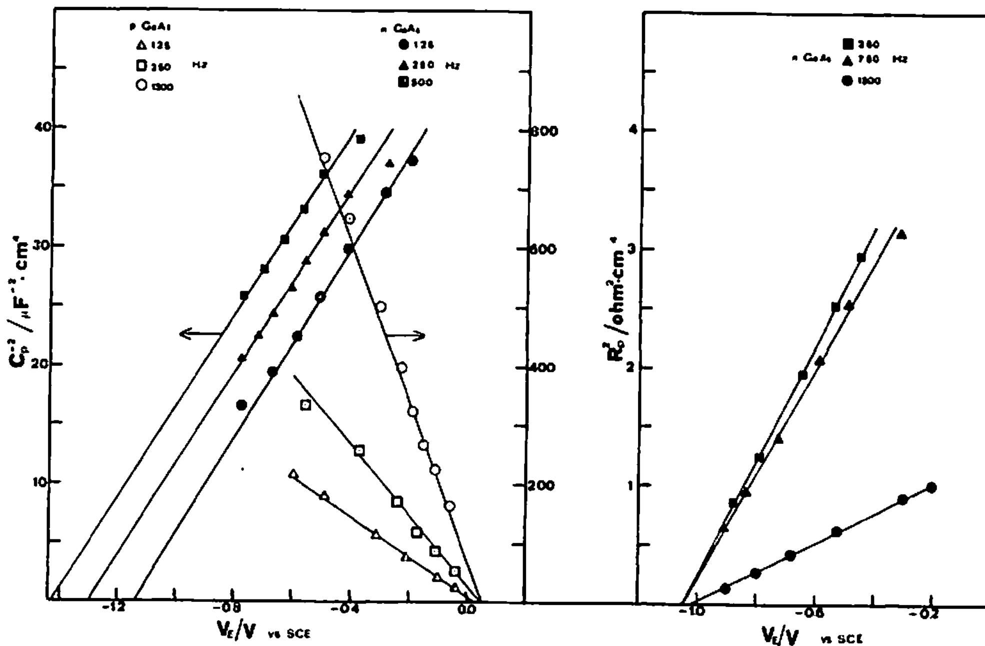

Fig. 1. Schottky–Mott plots and R_p^2 vs V plots in tetrahydrofuran–0.2 M TBAP. The values of R_p^2 are to be multiplied by 10^7 at 250 Hz; by 10^5 at 750 Hz; by 10^4 at 1500 Hz. R_p values shown have been corrected for solution resistance (2.6 ± 0.2 kΩ).

As concerns the effect of frequency on the S–M plots, we observed both a change in the slope at constant V-axis intersection and a change in the V-axis intersection at constant slope at different frequencies (see Fig. 1). Both of these effects were typical of the behavior of n-type electrodes, independent of the surface treatment. However, with p-type electrodes, the S–M plots at different frequencies usually showed the same V-axis intercept and little change in the slope. In some cases the S–M plots showed two linear portions of different slope, with the smaller one near the flat-band potential region.

At frequencies > 500 Hz for n-type and > 1.5 kHz for p-type, the C_p vs. V curves deviated from the usual behavior, and an increase in the measured C_p values was found with an increasing extent of band-bending. A more detailed analysis of the equivalent circuit suggested that this effect could be attributed to the presence of a series resistance consisting of the electrolyte resistance (2.6 ± 0.2 kΩ) and a space-charge resistance [11,23–25] which is frequency- as well as voltage-dependent. As shown previously [23–25], further information about the value of the flat-band potential can be obtained by investigating the frequency, as well as the voltage dependence, of the in-phase component of the impedance (in our case the measured quantity was the conductance $G_p = 1/R_p$). In G_p vs. V curves a decrease in the hysteresis was again observed when the potential range investigated was restricted. For n-type electrodes the G_p vs. V curves showed, at the lower frequencies, a minimum at more positive electrode potentials which disappeared at the higher frequencies ($f > 500$ Hz). Such behavior was absent in the p-type electrodes which showed a monotonic decrease of G_p with V over the potential range investigated. Lower G_p values were found for p-type electrodes, at the same frequency and extent of band-bending, as compared to the n-type electrodes. This can be attributed to the different doping levels for n- and p-type electrodes, the p-type electrode doping level was about an order of magnitude lower. As previously shown [11,23,25,26] plots of R_p^2 vs. V were straight lines for n-type electrodes. Moreover, for n-type electrodes the R_p^2 vs. V plots showed the same V-axis intercept, to within about ±100 mV, as the S–M plots obtained at the lowest frequencies (70–125 Hz). This was useful in estimating the flat-band potential for the n-type electrodes.

The impedance measurements thus yield the following estimated values for the flat-band potentials of the GaAs electrodes in these THF solutions: -1.0 ± 0.1 V (n-type) and 0.0 ± 0.1 V (p-type). Clearly, the observed results are also indicative of other effects which cause the frequency dispersion of C_p, etc. (e.g. surface films, frequency-dependent dielectric constants). However, a more complete study of the effects of surface treatment and frequency on the impedance is required before a more detailed model can be proposed.

Assignment of energy levels

From the slopes of the S–M plots a donor concentration $N_D = 3 \times 10^{17}$ cm^{-3} for n-type, and an acceptor concentration $N_A = 4 \times 10^{16}$ cm^{-3} for p-type electrodes was found. Both of these values are in good agreement with the doping levels reported by

the supplier. The CB of the n-type electrodes and the VB of the p-type electrodes can be located by use of the equations:

$$E_C - E_F = kT \ln(N_C/N_D) \quad \text{(n-type)} \tag{2a}$$

$$E_F - E_V = kT \ln(N_V/N_A) \quad \text{(p-type)} \tag{2b}$$

where E_F is the Fermi level of the semiconductor, E_C and E_V the energies of the edge of the CB and VB respectively and N_C and N_V the effective density of states in the CB and VB respectively.

For n-type electrodes at this doping level a more exact calculation [27], taking into account a possible slight degeneracy, does not produce an appreciable difference in the location of the CB edge. An effective density of states $N_C = 4.7 \times 10^{17}$ cm^{-3} and $N_V = 7.0 \times 10^{18}$ cm^{-3} has been assumed [28] so that from eqns. (2a) and

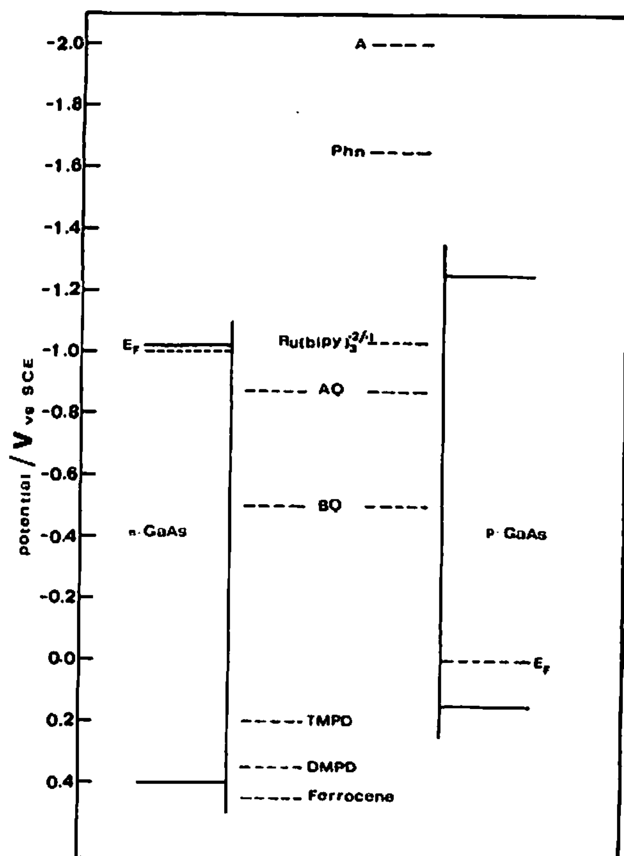

Fig. 2. Schematic representation of the energy levels at n- and p-GaAs/electrolyte interface. Abbreviations: (A) anthracene; (Phn) phthalonitrile; (bpy) bipyridine; (AQ) anthraquinone; (BQ) benzoquinone; (TMPD) *N,N,N′,N′*-tetramethyl-*p*-phenylenediamine; (DMPD) *N,N′*-dimethyl-*p*-phenylenediamine.

(2b) $E_C - E_F = 0$ eV and $E_F - E_V = 0.15$ eV. Since $E_F = -eV_{fb}$ and $E_C - E_V = E_g$, where E_g is the forbidden energy gap of the GaAs electrodes (1.4 eV at 300 K), a schematic picture of the energy levels for the n- and p-type GaAs/THF–TBAP interface can be given (Fig. 2). The band locations are based on estimates from the capacitance measurements, and, especially for the n-type electrodes, involve considerable uncertainty. Although the calculated results suggest an offset of the bands of the n- and p-type materials of ~0.2 V, as depicted in Fig. 2, the difference is within the reported uncertainties of the measurements, so that no actual offset of the bands of n- and p-type GaAs is necessarily present.

The estimated energy levels of the different redox couples, used in this work, based on the measured redox potentials at a Pt electrode, are also shown. The redox potential for each couple was taken as the mean of the anodic peak potential, E_{pa}, and the cathodic potential, E_{pc}, in cyclic voltammetric experiments.

Voltammetric studies

In the absence of redox couples, the range of stability of the solvent/electrolyte system at Pt electrodes was about +1.3 to −2.6 V vs. SCE. The cathodic limit was more negative at the semiconductor electrodes, and an apparent crystal dissolution process occurred in the dark with both n- and p-type electrodes before the anodic limit for stability was reached.

n-GaAs

On the basis of the ideal model of the interface [22] and the energy levels in Fig. 2, one would not expect any anodic faradaic current for couples which are located near or below the VB edge (e.g. ferrocene, TMPD, DMPD) except at very high doping levels and/or very positive potentials.

The experimental results reported in Figs. 3 and 4 are largely in agreement with this model. In fact, in the dark only a very small anodic current was observed for these couples up to a potential of about 0.3 V vs. SCE, where the anodic current started to increase. In the reversal scan a small cathodic peak was observed when the anodic scans were taken to potentials where appreciable anodic currents were observed. Under illumination, significant photocurrents were obtained which started well negative of the E_{pa} found on Pt. A distinct oxidation peak was observed only with DMPD, while a plateau with subsequent crystal oxidation was recorded in the presence of ferrocene and TMPD. A broad reduction peak under continuous illumination was also observed for these couples, but under chopped illumination a back-reaction during the dark period was visible only for the experiments in the presence of DMPD and ferrocene. In all cases a cathodic current was observed at electrode potentials more positive than V_{fb} (i.e. in the presence of an upward band-bending for n-type electrodes).

At the end of the experiments with TMPD and ferrocene, a surface layer appeared to be present on the electrode surface (observed by optical microscopy or visually without magnification). By washing with acetone, the layer lost its metallic

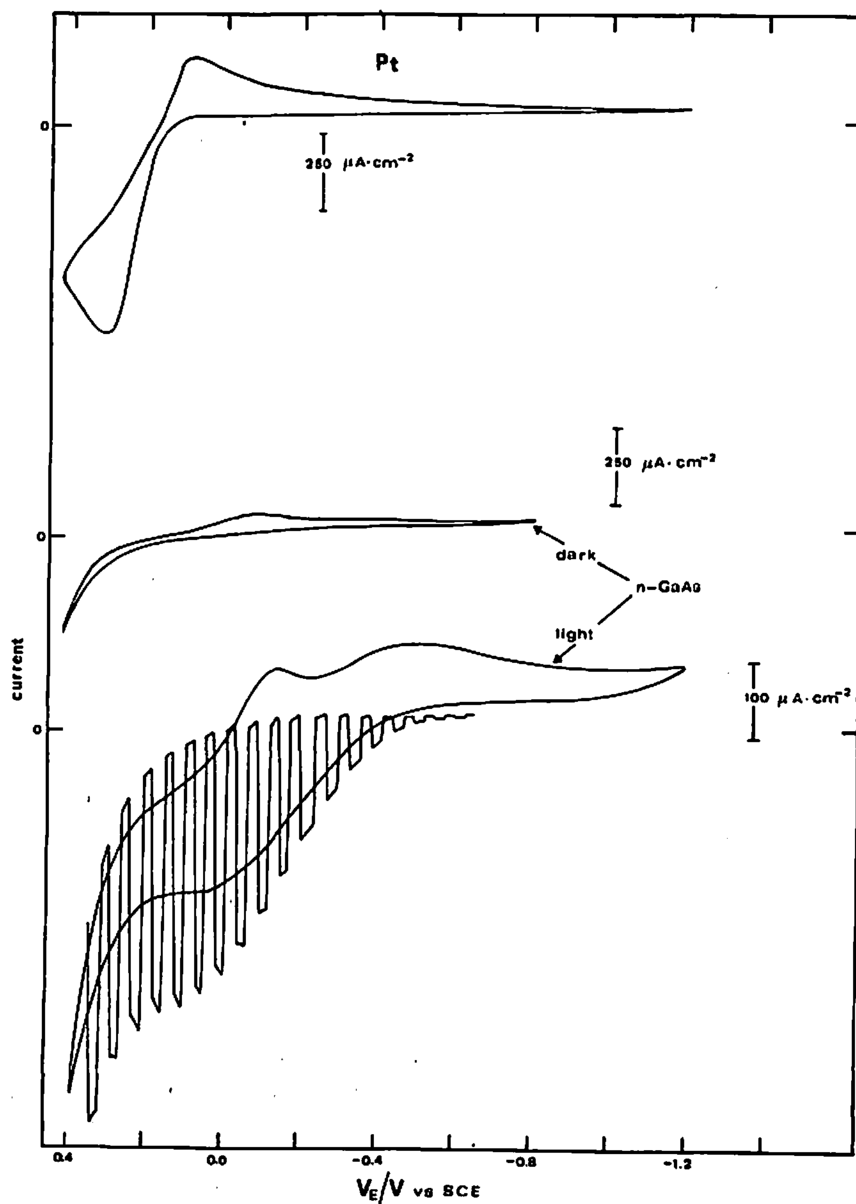

Fig. 3. Cyclic voltammograms of 10^{-2} *M* TMPD in THF–TBAP at a Pt disk electrode and single crystal n-GaAs electrode in the dark and illuminated with red light. The scan rate was 100 mV s^{-1} (Pt and GaAs in the dark). Under illumination the scan rate was 50 mV s^{-1}.

luster and became opaque. Immersion in $NH_3:H_2O$ (1 : 1) or in acidic solutions (pH 2.5) did not dissolve the layer. Anodization in H_3PO_4 solution (pH = 2.5) up to 100 V and subsequent etching in $NH_3:H_2O$ (1:1) caused the opaque layer to

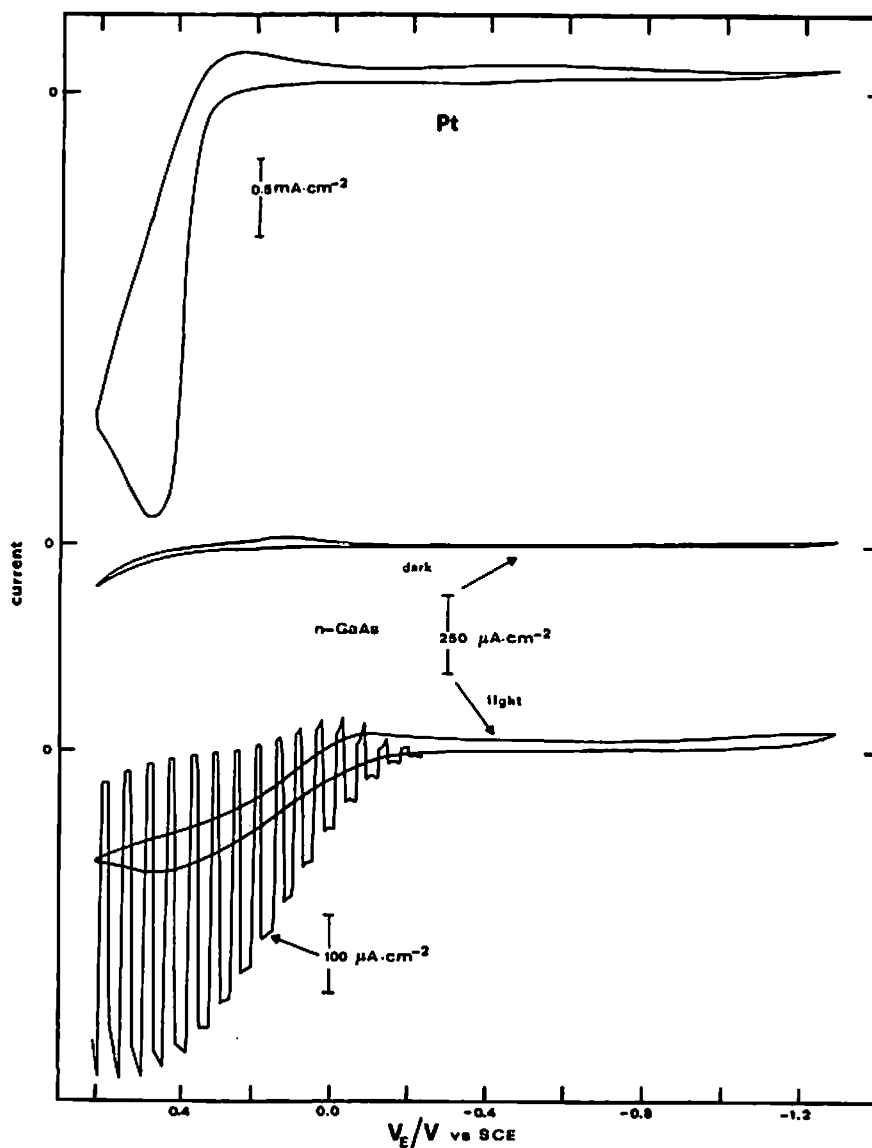

Fig. 4. Cyclic voltammograms of 2.5×10^{-2} *M* DMPD in THF–TBAP at a Pt disk electrode and single crystal n-GaAs electrode in the dark and illuminated with red light. The scan rate was 100 mV s^{-1} except for the chopped light experiment performed at 50 mV s^{-1}.

disappear and the electrode surface became highly reflecting. No further investigation of the identity or nature of these surface layers was attempted, but it seems very reasonable to correlate their appearance with the dissolution process of the electrode which occurs at high positive potentials and under illumination. Similar findings are

reported in the literature for investigations performed in aqueous solutions where the formation of a surface layer of cathodically deposited GaAs has been reported [7,8]. Such a suggestion is consistent with the stability of these layers both in acidic and in basic solutions, as well as with the absence of these layers on p-type electrodes (see below).

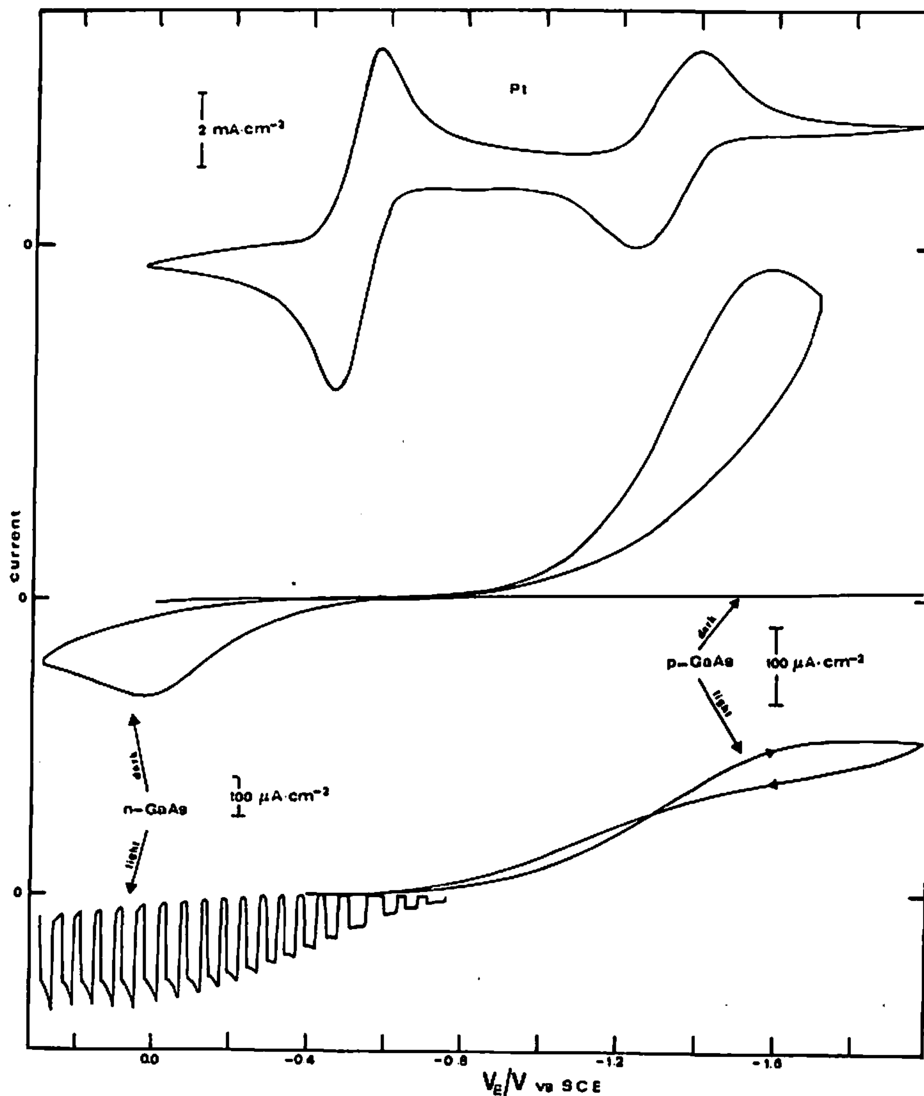

Fig. 5. Cyclic voltammograms of BQ in THF–TBAP at a Pt disk electrode and at n- and p-GaAs single crystal electrodes in the dark and illuminated with red light. The scan rate was 100 mV s^{-1}, except under illumination when it was 50 mV s^{-1}. The BQ concentration was 10^{-2} M in the experiments with n-GaAs and 5×10^{-3} M in the experiments with p-GaAs and Pt electrodes. The initial concentration of $BQ^{\cdot-}$ was 3×10^{-4} M.

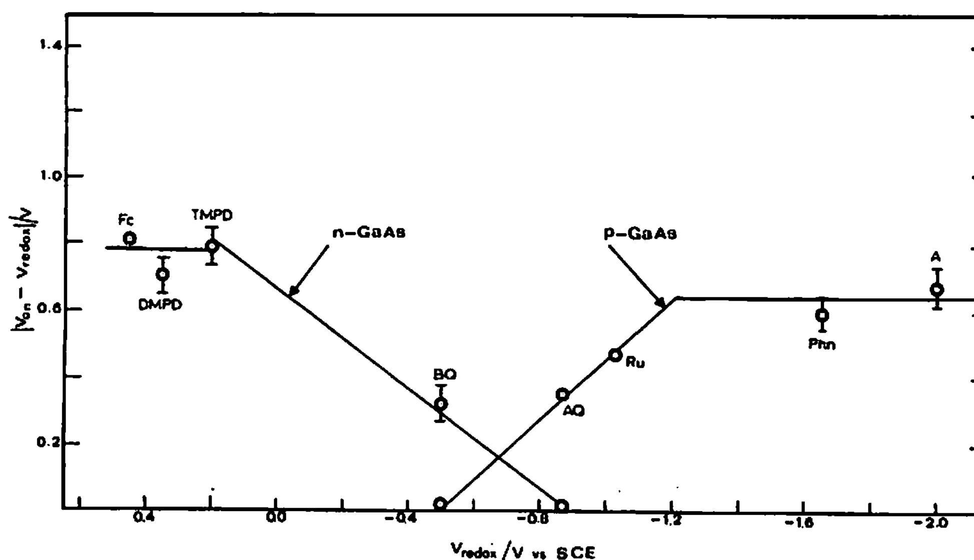

Fig. 6. The photovoltage as a function of the standard potentials of the redox couples. $V_{ph} = |V_{on} - V_{redox}|$.

The voltammetry of AQ and BQ at n-GaAs electrodes (see Fig. 5), showed a dark reduction of these species at potentials more negative than V_{fb}. An oxidation peak was observed in the dark for these redox couples following the cathodic scan at electrode potentials more positive than those for radical anion oxidation at a Pt disk electrode. Under illumination appreciable anodic photocurrents were observed, with both couples commencing near V_{fb}. Because V_{redox} for AQ is near V_{fb}, an underpotential was found only with BQ. No cathodic photoeffect was observed with AQ. A variable cathodic photoeffect, which depended on the previous history of the electrode, was observed with BQ. In this case a decrease in the cathodic current was recorded during the light-on period. A surface layer similiar to that previously described was also found in some cases in experiments with BQ.

The open-circuit photovoltage, V_{oc}, of photovoltaic cells with the different redox couples was very dependent on the past history of the electrodes. However, in general the experimental V_{oc} values were larger for the couples with V_{redox} values, corresponding to energies located far from the CB edge, as expected.

A more reliable parameter was the onset photopotential, defined as the electrode potential at which the photocurrents of the photoanodic waves start. In Fig. 6 the photovoltage $V_{ph} = V_{on} - V_{redox}$ is shown as a function of the standard potential of the couple. The plot shows a slope which is roughly equal to 0.8 for redox couples located in the band gap, and a zero slope for couples located near the edge or below the VB of the n-GaAs electrodes.

p-GaAs

The voltammetric behavior of p-GaAs electrodes in the presence of redox couples

lying within the band-gap region or above the CB edge generally showed the absence of oxidation or reduction peaks in the dark and the presence of a strong photoeffect under illumination, even for couples located well above the CB. The first aspect is in agreement with the ideal behavior of a p-type semiconductor when held at potentials which are more negative than V_{fb}. The electrode potential was scanned between 0.0 and −2.2 V vs. SCE with all redox couples in these experiments. No oxidation current would be expected for electron transfer between reduced species in solution and positive holes coming from the VB for these couples. Similarly, the absence of a dark reduction current can be attributed to the absence of an appreciable electron concentration in the CB with the p-type semiconductor. Neither would appreciable direct tunnelling of electrons from the VB be expected in this case because of the low doping level of these p-GaAs electrodes.

The existence of a photoeffect in the presence of anthracene ($V_{redox} = -1.97$ V vs. SCE) and phthalonitrile ($V_{redox} = -1.65$ V vs. SCE) which are both located above the CB edge is analogous to the behavior of n-GaAs in the presence of couples located below the VB edge.

As shown in Figs. 7 and 8, only very low currents were observed in the dark with both of these couples for electrode potentials between −0.3 and −2.2 V vs. SCE. However, under illumination both cathodic and anodic peaks were observed in the presence of the $A/A^{\cdot-}$ couple, while a somewhat less well-developed wave was observed with the phthalonitrile redox couple. A distinct anodic peak was also observed with the $A/A^{\cdot-}$ couple when the anodic scan was performed in the dark immediately after a cathodic scan taken under continuous or chopped illumination (see dashed curve in Fig. 7). Although this effect was observed in the presence of phthalonitrile, it was less distinct. Note also the existence of a noticeable back-reaction during the dark period in the presence of the $A/A^{\cdot-}$ couple in the experiments performed with chopped light.

In the presence of couples located within the band-gap region [AQ, BQ, $Ru(bpy)_3^{2+}$], the underpotential in the cathodic wave at p-GaAs under illumination depended on the V_{redox} of the couples. As shown in Fig. 6, V_{ph}, defined as $V_{ph} = |V_{on} - V_{redox}|$, was zero for BQ, and increased linearly with V_{redox} for AQ and $Ru(bpy)_3^{2+}$. A plot of V_{ph} vs. V_{redox} for AQ and $Ru(bpy)_3^{2+}$. A plot of V_{ph} vs. V_{redox} has a slope of about 0.9 for couples lying below the CB edge, and saturates at ~0.6 V for couples located above the CB edge.

Although these couples showed well-developed cathodic and anodic peaks on a Pt disk electrode [$Ru(bpy)_3^{2+}$ showed only one well-shaped anodic peak], under illumination at p-GaAs the cathodic and anodic waves were drawn out, with no clear peaks. In some cases [BQ, $Ru(bpy)_3^{2+}$] in the dark and under illumination (BQ), the reversal voltammetric scan overlapped the forward one.

As opposed to the results with the n-type electrode, no surface layers were found at the end of the experiments performed under illumination with the p-type materials. For photovoltaic cells an open-circuit photovoltage was found with all redox couples, 0.06 V with BQ, 0.35 V with $Ru(bpy)_3^{2+}$, and ~0.2 V with A. As with n-GaAs the exact value of V_{oc} depended upon the detailed past history of the electrode.

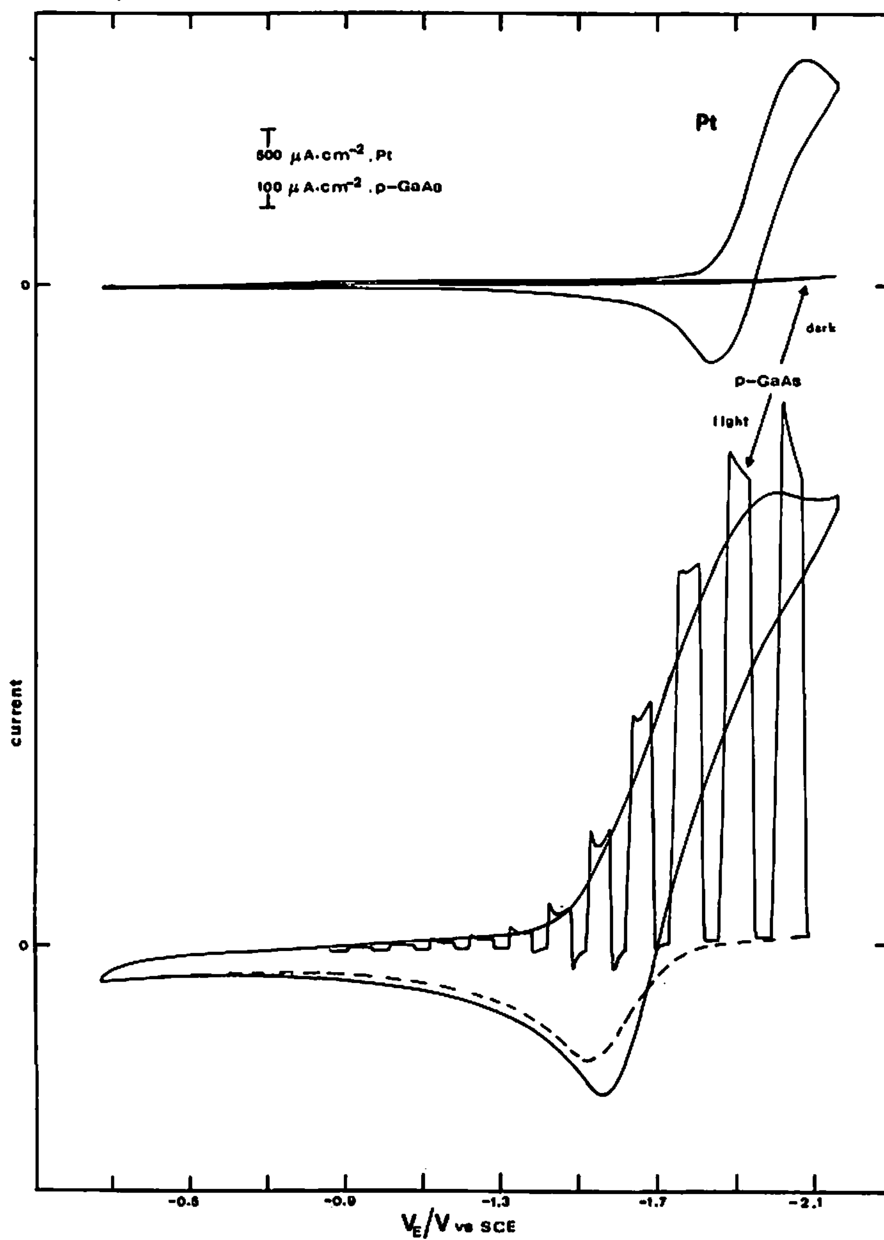

Fig. 7. Cyclic voltammograms of 6×10^{-3} *M* anthracene in THF–TBAP at a Pt disk electrode and single crystal p-GaAs electrode in the dark and illuminated with red light. The dashed curve represents the reversal scan in the dark following the forward one which was performed under chopped illumination. The scan rate was 100 mV s^{-1}.

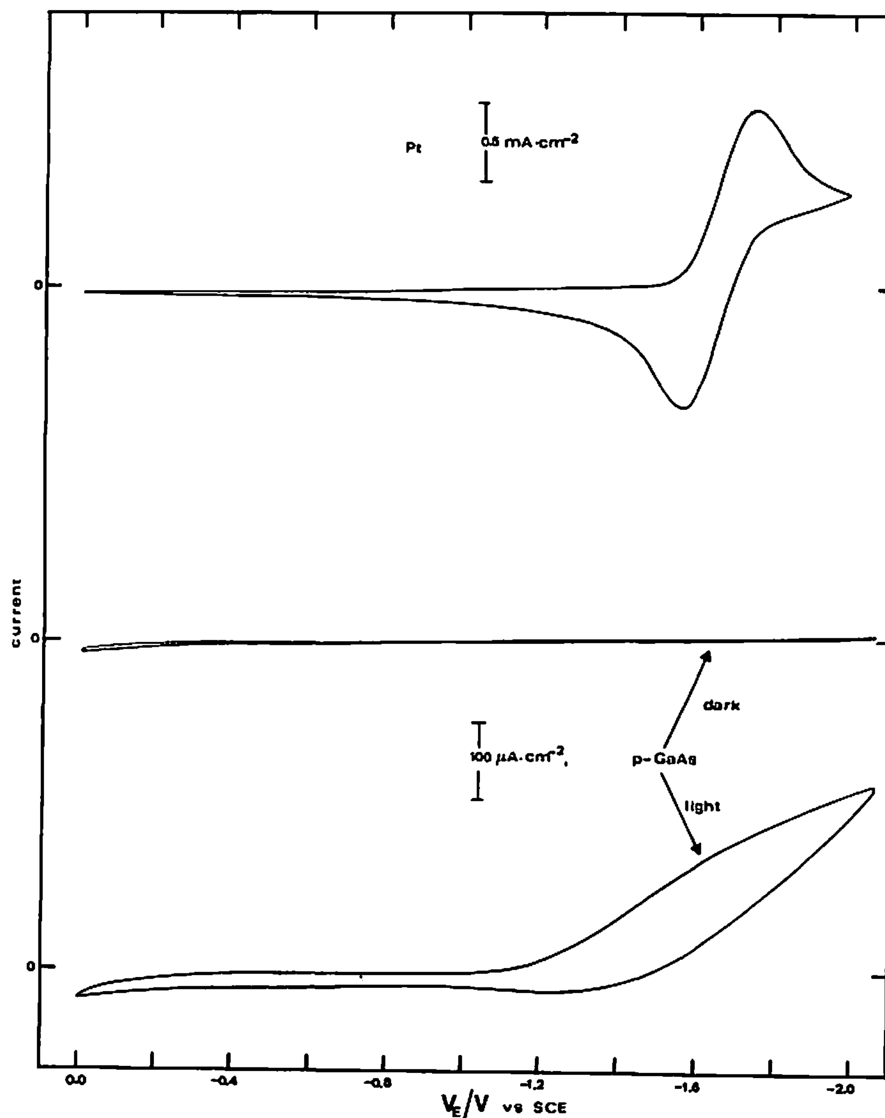

Fig. 8. Cyclic voltammograms of 4.6×10^{-3} *M* of phthalonitrile at a Pt disk electrode and single crystal p-GaAs electrode in the dark and illuminated with red light. The scan rate was 100 mV s^{-1}.

DISCUSSION

The behavior of n- and p-type GaAs is, in many ways, analogous to that found recently with n- and p-type WSe_2 in acetonitrile solutions [29,30]. The plot of V_{ph} vs. V_{redox} shows a linear increase with a slope approaching, but less than, unity. V_{ph} attains a limiting value of the order of half of that corresponding to E_g at potentials

near V_{fb} for both materials. Moreover, as observed previously with p- and n-WSe_2 [29–31], p-GaAs [17,32,33], p-Si [32,34], and n- and p-InP [35–37], photoeffects are observed for redox couples located below the VB edge (n-type) and above the CB edge (p-type). This type of behavior has been attributed to either Fermi-level pinning [32] or inversion [31]. In both of these processes the accumulation of charge at the surface of the semiconductor causes a change in the potential drop across the Helmholtz layer, which is equivalent to a shift in the position of the semiconductor bands with respect to the redox levels in solution. The fact that the onset of photovoltage saturation takes place at V_{redox} values near the band edges suggests that inversion occurs, although a high density of surface states localized at energies near the band edges would show a similar effect. The existence of such surface states is suggested by the less than unity slope of the $V_{ph}-V_{redox}$ plot which can be attributed to recombination effects [33]. Moreover, the intersection of the lines with the V_{redox} axis occurs at potentials well negative of V_{fb} for p-type, and slightly positive of V_{fb} for n-type. For example, the lack of an appreciable photoeffect with BQ on p-GaAs, although it is located energetically near the middle of the gap, may be attributable to recombination mediated by a moderate density of states at the p-type material surface. A similar explanation can be invoked for AQ at n-GaAs, although the proximity of the CB edge to V_{redox} ($\sim$0.1–0.2 V) would lead to only a small photoeffect in any case.

CONCLUSIONS

The photoelectrochemical behavior of p- and n-GaAs in THF/TBAP solutions generally parallels that found in acetonitrile. The surface-state pinning effect on p-GaAs, noted in both aqueous and acetonitrile solutions, is less pronounced in THF. Photoeffects at n- and p-GaAs occur over a potential range of 2.4 eV, which is much larger than the band-gap energy of 1.4 eV. These photo-oxidations which occur below the VB edge on n-GaAs and reductions above the CB edge on p-GaAs can be attributed to the onset of inversion or pinning by localized states near the band edges.

ACKNOWLEDGEMENT

The support of this research by the Solar Energy Research Institute (in a cooperative project with SumX Corporation) is gratefully acknowledged.

REFERENCES

1 A.J. Bard and P.A. Kohl in A. Heller (Ed.), Semiconductor Liquid-Junction Solar Cells, Electrochemical Society, Princeton, N.J. (Proceedings, Vol. 77-3) 1977, p. 222.
2 S.N. Frank and A.J. Bard, J. Am. Chem. Soc., 97 (1975) 7427.
3 A.J. Bard and M.S. Wrighton, J. Electrochem. Soc., 124 (1977) 1706.
4 H. Gerischer, J. Electroanal. Chem., 82 (1977) 133.
5 Yu.V. Pleskov, Dokl. Akad. Nauk., 143 (1962) 1309.

6 H. Gerischer and I. Mattes, Z. Phys. Chem., 49 (1966) 112.
7 H. Gerischer, Ber. Bunsenges. Phys. Chem., 69 (1965) 578.
8 W.W. Harvey, J. Electrochem. Soc., 114 (1967) 472.
9 K.D.N. Brummer, J. Electrochem. Soc., 114 (1967) 1274.
10 S.A. Molchanova, Zh. Fiz. Khim., 45 (1971) 959.
11 W.H. Laflere, R.C. Van Meirhaeghe, F. Cardon, Surf. Sci., 59 (1976) 401.
12 K.C. Chang, A. Heller, B. Schwartz, S. Menezes and B. Miller, Science, 196 (1977) 1097.
13 A. Heller and B. Miller, Electrochim. Acta, 25 (1980) 29.
14 A.B. Ellis, J.M. Bolts, S.W. Kaiser and M.S. Wrighton, J. Am. Chem. Soc., 99 (1977) 2848.
15 P.A. Kohl and A.J. Bard, J. Am. Chem. Soc., 99 (1977) 7531.
16 P.A. Kohl, S.N. Frank and A.J. Bard, J. Electrochem. Soc., 125 (1978) 246.
17 P.A. Kohl and A.J. Bard, J. Electrochem. So., 126 (1979) 59.
18 P.A. Kohl and A.J. Bard, J. Electrochem. Soc., 126 (1979) 598.
19 J.T. Law in B. Hannay (Ed.), Semiconductors, Reinhold, New York, 1959, p. 676.
20 A. Many, Y. Goldstein and N.B. Grover, in Semiconductor Surfaces, North-Holland, Amsterdam, 1971.
21 C.C. Chang, P.H. Citrin and B. Schwartz, J. Vac. Sci. Technol., 14 (1977) 943.
22 H. Gerischer in P. Delahay and C.W. Tobias (Eds.), Advances in Electrochemical Engineering, Vol. I, Interscience, New York, 1961, p. 139.
23 V.A. Tyagai, Izv. Akad. Nauk S.S.S.R., Ser. Khim., (1964) 34.
24 V.A. Myamlin and Yu.V. Pleskov in Electrochemistry of Semiconductors, Plenum Press, New York, 1967, p. 323.
25 E.C. Dutoit, R.L. Van Meirhaeghe, F. Cardon and W.P. Gomes, Ber. Bunsenges. Phys. Chem., 79 (1975) 1206.
26 J.L. Sculfort and A.M. Baticle, Surf. Sci., 85 (1979) 137.
27 J.S. Blakemore in Semiconductor Statistics, Pergamon Press, Oxford, 1962, p. 82.
28 S.M. Sze in Physics of Semiconductor Devices, Wiley, New York, 1967, p. 22.
29 H. White, F.R. Fan and A.J. Bard, J. Electrochem. Soc., 128 (1981) 1045.
30 G. Nagasubramanian and A.J. Bard, J. Electrochem. Soc., 128 (1981) 1055.
31 W. Kautek and H. Gerischer, Ber. Bunsenges. Phys. Chem., 84 (1980) 645.
32 A.J. Bard, A.B. Bocarsly, F-R.F. Fan, E.G. Walton and M.S. Wrighton, J. Am. Chem. Soc., 102 (1980) 3671.
33 F-R.F. Fan and A.J. Bard, J. Am. Chem. Soc., 102 (1980) 3677.
34 A.B. Bocarsly, D.C. Bookbinder, R.N. Dominey, N.S. Lewis and M.S. Wrighton, J. Am. Chem. Soc., 102 (1980) 3683.
35 J.D. Luttmer and A.J. Bard, J. Electrochem. Soc., 126 (1979) 414.
36 P.A. Kohl and A.J. Bard, J. Electrochem. Soc., 126 (1979) 698.
37 R.N. Dominey, N.S. Lewis and M.S. Wrighton, J. Am. Chem. Soc., 103 (1981) 1261.